A combined wind wave–tidal model for the Venice lagoon, Italy

L. Carniello and A. Defina
Department of Hydraulic, Maritime, Environmental and Geotechnics Engineering, University of Padua, Padua, Italy

S. Fagherazzi
Department of Geological Sciences and School of Computational Science and Information Technology, Florida State University, Tallahassee, Florida, USA

L. D'Alpaos
Department of Hydraulic, Maritime, Environmental and Geotechnics Engineering, University of Padua, Padua, Italy

Received 30 August 2004; revised 8 March 2005; accepted 1 June 2005; published 27 October 2005.

[1] A numerical model that combines wind waves with tidal fluxes in a tidal basin is presented and validated. The model couples a hydrodynamic finite element module based on the shallow water equations with a finite volume module that accounts for the generation and propagation of wind waves. The wave module solves the wave action conservation on the same triangular mesh used in the hydrodynamic module, thus efficiently reproducing the physical relationships between waves and tide propagation. The combined wind wave–tidal model is applied to the Venice lagoon, Italy. The highly irregular bathymetry of this tidal environment, characterized by deep channels, emergent salt marshes, and extensive tidal flats, suggests the introduction of specific hypotheses that simplify the governing equations with a noteworthy increase in efficiency and robustness of the algorithm. Particular attention is devoted to the dissipation of wave energy at the steep boundaries between channels, tidal flats, and salt marshes. Simulations of wave fields generated under specific wind conditions are presented and discussed. The model results are compared, with good agreement, to field data collected in different stations inside the lagoon of Venice. Finally, evidence of the complementary effect of tidal currents and wind waves on bottom shear stresses is presented using the results of different simulations.

Citation: Carniello, L., A. Defina, S. Fagherazzi, and L. D'Alpaos (2005), A combined wind wave–tidal model for the Venice lagoon, Italy, *J. Geophys. Res.*, *110*, F04007, doi:10.1029/2004JF000232.

1. Introduction

[2] The lagoon of Venice is a wide, shallow tidal basin in the northeast of Italy. A large part of the lagoon is occupied by small islands and extensive tidal flats, which are dissected by an intricate network of channels departing from the three inlets of Lido, Malamocco, and Chioggia (Figure 1, see also *Fagherazzi et al.* [1999] for a description).

[3] Recent studies and field campaigns have shown that the salt marshes and tidal flats within the Venice lagoon are under erosion with a net sediment loss for the entire tidal basin [*Day et al.*, 1999; *Bettenetti et al.*, 1995, *D'Alpaos and Martini*, 2003; *Martini et al.*, 2003]. A further important trend within the lagoon is the flattening of the bottom topography, as proved by the gradual but persistent reduction of salt marshes and by the silting of the tidal channels. This trend is further enhanced by subsidence and sea level rise.

0148-0227/05/2004JF000232$09.00

[4] Because of the above considerations it is clear that a correct description of local sediment resuspension is very important in understanding and assessing the evolution trend of the Venice lagoon.

[5] Tidal currents alone are unable to explain the erosion of salt marshes and the flattening of the lagoon bottom. Tidal currents produce shear stresses large enough to carry sediments into suspension only in the large channels near the three inlets, where velocities are high. In contrast, sediment resuspension on salt marshes and tidal flats is mainly caused by shear stresses induced by wind waves.

[6] Since shallow tidal basins have a very irregular morphology with large and sudden changes in bottom elevation, islands, and temporarily dry areas, a specific framework must be adopted to model wind wave propagation in these environments.

[7] Two alternative methods are available to model wind wave generation and propagation, i.e., a phase-resolving approach, based on mass and momentum balance equations (for a review, see *Dingemans* [1997]); or a phase-averaged

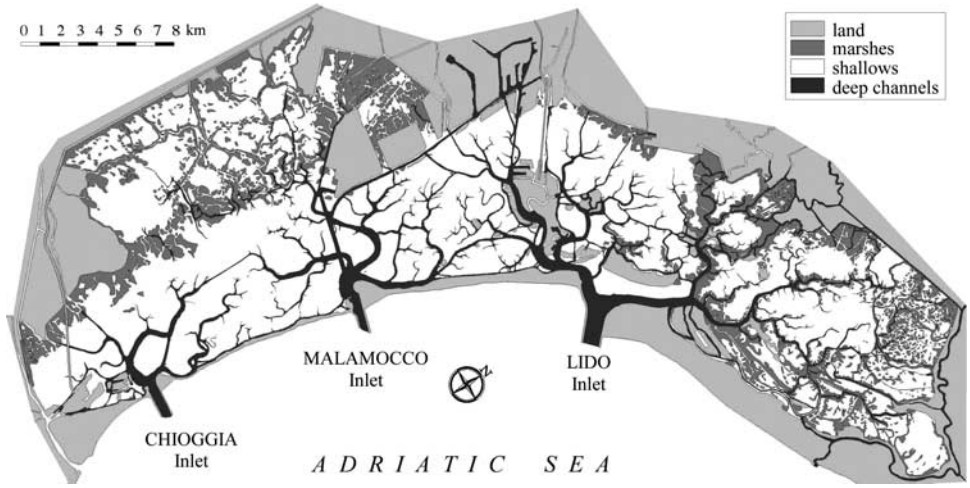

Figure 1. Lagoon of Venice, Italy.

approach that solves the energy or action balance equation [e.g., *Booij et al.*, 1999].

[8] Phase-resolving models reproduce the sea surface in space and time accounting for effects such as refraction and diffraction. Bottom friction and depth-induced wave breaking can be included in this framework but wind wave generation is usually absent or poorly reproduced. Phase-resolving models are thus unsuitable in enclosed basins, where storm conditions are important and local wave generation is a key process. Furthermore the space and time resolutions required by phase-resolving models are of the order of a fraction of the wavelength and period, respectively, thus limiting their practical application to small domains and short-duration events.

[9] For large-scale applications, such as for the modeling wind waves in the Venice lagoon, phase-averaged models are more suitable. There are two commonly used approaches to implement these models, i.e., the Lagrangian approach transporting wave energy along rays [*Collins*, 1972; *Cavaleri and Malanotte-Rizzoli*, 1981] and the Eulerian approach, where the wave energy is convected among cells of a prescribed computational grid. The latter is more efficient when nonlinear effects such as wave breaking must be reproduced.

[10] In the Eulerian approach the energy balance leads to a convective equation in which all the relevant processes of wave generation and dissipation are included in the source term.

[11] Many models that use the Eulerian phase-averaged approach have been developed since the pioneering work of *Gelci et al.* [1956]. Among them, the GLERL model developed by *Donelan* [1977] and revised by *Schwab et al.* [1984] for Great Lakes wave prediction, deserves to be mentioned here. GLERL is based on the solution of the local momentum balance equations, is time-dependent and can be applied to arbitrary bathymetries and wind conditions. However, shallow water wave effects are not included in this model.

[12] A successful extension of deep-water wave models to finite depth domains are the Hindcast Shallow water Waves model (HISWA model [see *Holthuijsen et al.*, 1989]), and its successor the Simulating Wave Nearshore (SWAN) model [*Booij et al.*, 1999; *Ris et al.*, 1999]. These models solve the wave action conservation equation using an implicit finite difference numerical scheme. The SWAN model accounts for refraction, shoaling, and wave breaking, and explicitly represents nonlinear wave-wave interactions.

[13] Further shallow water wave models are the WAVAD model [*Resio*, 1987; *Resio and Pierre*, 1989], and the Automated Coastal Engineering System (ACES) model, empirically derived from limited field data sets using dimensional analysis [*Leenknecht et al.*, 1992].

[14] *Lin et al.* [1998] tested all the models mentioned above against a wind and wave data set collected in the northern Chesapeake Bay during September 1992, when the tropical storm Danielle passed over the area. They found that no single model seems to be good at predicting all aspects of the surface wave field in the Chesapeake Bay, but the GLERL and SWAN models were the most promising. A further comparison of these two models against a more complete wind and wave data set collected in Chesapeake Bay is presented by *Lin et al.* [2002]. Both SWAN and GLERL correctly reproduce the change in wave direction due to a sudden wind variation. The models overpredict significant wave height (SWAN overpredicts more than GLERL does) and both underpredict the peak period. Using the SWAN model, *Lin et al.* [2002] also performed a model data spectral analysis that supported what was found in the previous comparison.

[15] The above discrepancies between measured and modeled waves will be enhanced in a shallower and more irregular basin like the Venice lagoon. In particular, in Chesapeake Bay there are not the deep channels, the extensive salt marshes, and the islands typical of the Venice lagoon. Moreover, Chesapeake Bay is deep enough (average water depth of 8.5 m against a depth of approximately 1 m in the Venice lagoon) to prevent the emergence of tidal flats during low tide.

[16] Even though the evaluation of nonlinear terms as triad interactions is important for the calculation of wave spectra in shallow waters, the SWAN model is in better agreement with shallow water flume experiments when the triad interactions are neglected [see *Wood et al.*, 2001; *Feola*, 2002].

[17] The detailed calculation of the spectral evolution of wind waves is also computationally expensive [see *Lin et al.*, 2002] thus hindering the applicability of these models to midterm and long-term studies.

[18] Moreover, the instantaneous value of the local water depth is crucial to correctly predict the wave field, since water depths strongly affects wave propagation. Wave prediction can therefore be accomplished only by coupling a hydrodynamic model with a wave model.

[19] A recent attempt to couple a hydrodynamic model with a wave model for the Venice lagoon was made by *Umgiesser et al.* [2002, 2004]. They combined a two-dimensional finite elements model [*Umgiesser and Bergamasco*, 1993] with the finite difference SWAN model run in stationary mode. The hydrodynamic model uses an unstructured mesh reproducing the Venice lagoon comprising 4359 nodes and 7845 triangular elements and a grid size ranging from 50m to 1 km. The SWAN model uses a 100 m regular grid. For consistency, all the results produced by the hydrodynamic model are interpolated to the grid of the wave model, thus introducing significant numerical approximations. It is also worth noting that the coarse grid used by *Umgiesser et al.* [2004] does not allow for an accurate resolution of wave refraction.

[20] Given the irregular bathymetry of the Venice lagoon and the uncertainties affecting the modeling of non linear wave interactions, a simplified, computationally efficient model, which propagates a monochromatic wave, is presented herein. The model reproduces the wind wave generation and propagation inside the lagoon of Venice by solving the wave action conservation equation on an unstructured triangular mesh of arbitrary shape with a first-order finite volume explicit scheme. The wave model is coupled with a hydrodynamic model for tide propagation inside the basin based on a finite element scheme [*D'Alpaos and Defina*, 1995]. Both models share the same computational grid, enabling us to accurately reproduce irregular domains and to correctly account for the interactions between waves and tides. In the model special attention is given to describing all the physical phenomena producing or dissipating wave energy. Wind waves are then combined to tidal currents in order to determine bottom shear stresses necessary to describe erosion patterns in tidal basins.

[21] Numerical simulations reproducing the wind wave field inside the Venice lagoon under different wind and tidal conditions are presented and the results are compared with recent data collected in two field stations. Finally, bottom shear stress distributions are evaluated to assess the potential for sediment resuspension in shallow tidal basins due to the combined action of tidal currents and wind waves.

2. Tidal Model

[22] The hydrodynamic model solves the two-dimensional shallow water equations modified to deal with flooding and drying processes in very irregular domains. On the basis of the idea that refined subgrid modeling of bathymetric data could lead to a physically consistent, and "universal" (i.e., not dependent on the numerical technique) solution of the wetting and drying problem, a new set of two dimensional shallow water equations was developed [*Defina et al.*, 1994; *D'Alpaos and Defina*, 1995; *Defina*, 2000].

[23] The presence of bottom irregularities, which strongly affect the dynamics and the continuity in very shallow flows, is considered in the model from a statistical point of view. Assuming the hydrostatic approximation, the three dimensional Reynolds equations are suitably averaged over a representative elementary area (REA) and then integrated over the depth. The resulting subgrid model for ground irregularities proves to be very effective in the simulation of tide propagation in shallow lagoons.

[24] The averaged equations are

$$\frac{\partial q_x}{\partial t}+\frac{\partial}{\partial x}\left(\frac{q_x^2}{Y}\right)+\frac{\partial}{\partial y}\left(\frac{q_x q_y}{Y}\right)-\left(\frac{\partial R_{xx}}{\partial x}+\frac{\partial R_{xy}}{\partial y}\right)+\frac{\tau_{bx}}{\rho}-\frac{\tau_{wx}}{\rho}+g\,Y\,\frac{\partial h}{\partial x}=0 \tag{1}$$

$$\frac{\partial q_y}{\partial t}+\frac{\partial}{\partial x}\left(\frac{q_x q_y}{Y}\right)+\frac{\partial}{\partial y}\left(\frac{q_y^2}{Y}\right)-\left(\frac{\partial R_{xy}}{\partial x}+\frac{\partial R_{yy}}{\partial y}\right)+\frac{\tau_{by}}{\rho}-\frac{\tau_{wy}}{\rho}+g\,Y\,\frac{\partial h}{\partial y}=0 \tag{2}$$

$$\eta\,\frac{\partial h}{\partial t}+\frac{\partial q_x}{\partial x}+\frac{\partial q_y}{\partial y}=0 \tag{3}$$

where t denotes time, q_x, q_y are the flow rates per unit width in the x, y (planform) directions respectively, R_{ij} are the Reynolds stresses (i, j denoting either the x or y coordinates), $\boldsymbol{\tau}_{b,\mathrm{curr}} = (\tau_{bx}, \tau_{by})$ is the stress at the bottom produced by the tidal current, $\boldsymbol{\tau}_w = (\tau_{wx}, \tau_{wy})$ is the wind shear stress at the free surface, ρ is fluid density, h is the free surface elevation, g is gravity. Y is the equivalent water depth, defined as the volume of water per unit area actually ponding the bottom, η is the local fraction of wetted domain which can be interpreted as an h-dependent storativity coefficient (similar to the one used in groundwater hydraulics), accounting for the actual area that can be wetted or dried during the tidal cycle.

[25] Further assuming that bottom elevations in the REA are distributed according to a Gaussian probability density function, the functions η and Y are found to be [*Defina*, 2000]

$$\eta=\frac{1}{2}\left\{1+\mathrm{erf}\left[\frac{2D}{a_r}\right]\right\} \tag{4}$$

$$Y=a_r\left\{\eta\,(D/a_r)+\frac{1}{4\sqrt{\pi}}\exp\left[-4\,(D/a_r)^2\right]\right\} \tag{5}$$

where erf( ) is the error function, a_r is the typical height of bottom irregularities (i.e., the maximum amplitude of bottom irregularities or, approximately twice the standard deviation of bottom elevations), $D = h - z_b$ is the average water depth, z_b being the average bottom elevation within a REA.

[26] For the case of a turbulent flow over a rough wall, the bed shear stress can be written as [*Defina*, 2000]

$$\frac{\tau_{b,\mathrm{curr}}}{\rho\, Y} = g\left(\frac{|\mathbf{q}|}{K_s^2 H^{10/3}}\right)\mathbf{q} \tag{6}$$

where $\mathbf{q} = (q_x, q_y)$, $|\mathbf{q}| = \sqrt{q_x^2 + q_y^2}$, K_s is the Strickler bed roughness coefficient, and H is an equivalent water depth which can be approximated with the following interpolation formula:

$$H/a_r \cong Y/a_r + 0.27\,\sqrt{Y/a_r}\; e^{-2\,Y/a_r} \tag{7}$$

The wind shear stress at the free surface $\boldsymbol{\tau}_w$, is evaluated as

$$\tau_w = \rho_a c_d U_{\mathrm{wind}}^2 \tag{8}$$

where ρ_a is the air density (1.25 kg/m^3), c_d is drag coefficient, and U_{wind} is wind speed. The model assumes a constant drag coefficient, i.e., $c_d = 0.001$ in accordance with *Smith and Banke* [1975] for a wind velocity ranging between 5 and 15 m/s. Moreover, in the present scheme, Reynolds stresses and convective terms are neglected.

[27] A semi-implicit staggered finite element method based on Galerkin's approach is used to implement the model [*D'Alpaos and Defina*, 1995; *Defina*, 2003]. This numerical scheme is very suitable when dealing with morphologically complicated basins such as the Venice lagoon.

[28] In the model, the surface elevation h is assumed to vary linearly between element nodes (i.e., p1 discretization) while the depth integrated velocity components q_x, q_y are assumed constant within each element (i.e., p0 discretization). At each time step, the hydrodynamic model yields nodal water levels which are used by the wind wave model to assess wave group celerity and bottom influence on wave propagation. Moreover, depth integrated velocity and water depth computed with the hydrodynamic model are used to evaluate the bottom shear stress produced by the combined action of tidal currents and wind waves.

3. Wind Wave Model

[29] The wind wave model is based on the conservation of the wave action N, which is defined as the ratio of wave energy E to the relative wave frequency σ.

[30] The wave action conservation equation, in the most general spectral formulation is [*Hasselmann et al.*, 1973]

$$\frac{\partial N}{\partial t} + \frac{\partial}{\partial x} c_{gx} N + \frac{\partial}{\partial y} c_{gy} N + \frac{\partial}{\partial \sigma} c_\sigma N + \frac{\partial}{\partial \vartheta} c_\vartheta N = \frac{S}{\sigma} \tag{9}$$

The first term of (9) represents the local rate of change of action density in time, the second and third terms represent the propagation of wave action in space (c_{gx} and c_{gy} are the x and y components of the wave group celerity). The fourth term represents shifting of the relative frequency σ due to variations in depth and currents. The fifth term represents depth-induced and current-induced refraction, θ being the wave direction). The source term S on the right-hand side of (9) includes wave growth by wind and wave decay by bottom friction, white capping, and depth-induced breaking.

[31] Some terms of equation (9) can be neglected by making some justifiable assumptions. Given the relatively poor performance of spectral models in shallow tidal basins [see *Lin et al.*, 2002], we prefer to utilize a monochromatic wave which allows for a noteworthy reduction of computational effort. This simplified approach is particularly suitable for long-term morphological studies, in which the simulated period is very long. The monochromatic wave assumption allows us to neglect the fourth term in (9). Moreover, according to linear wave theory, we consider the wave period T, and thus the wave frequency $\sigma = 2\pi/T$, constant during propagation. This simplification, combined with the monochromatic assumption, makes it possible to use the dispersion equation relating the wave number k ($k = 2\pi/\lambda$, λ being the wavelength) to the water depth Y:

$$\sigma = \sqrt{gk\tanh(kY)} \tag{10}$$

Moreover, the model assumes that the direction of wave propagation instantaneously readjusts to match the wind direction. This hypothesis is supported by the results of a numerical study on the decay of wave energy in the lagoon of Venice. Starting from a given wave field in equilibrium with the wind, we instantaneously reduce to zero the wind energy input and calculate the time required for wave height to decay due to bottom friction. Several experiments are performed by varying the flow depth, friction coefficient and wind velocity (i.e., equilibrium wave height). The results of these experiments show that wave height decays to 1% of its initial value in a time interval of approximately 5$\sim$10 min, which is a short time when compared to common wind durations, thus validating our assumption. The reliability of this hypothesis is enhanced by forcing the model with a wind field that has smooth changes in direction and speed by neglecting gusts that, in general, have a small impact on the generation of a stable wave field.

[32] Further evidence supporting the above hypothesis is given by *Lin et al.* [2002], who show that wind and wave data collected in the Chesapeake Bay indicate that the mean wave direction closely follows the wind direction.

[33] With the above assumption we implicitly neglect refraction. Indeed, it is basically impossible to correctly evaluate wave refraction in a very irregular domain with sharp and frequent discontinuities of the bottom, when using a comparably coarse grid.

[34] According to the above discussion the fifth term of the wave action conservation equation (9) can be neglected, thus obtaining

$$\frac{\partial N}{\partial t} + \frac{\partial}{\partial x} c_{gx} N + \frac{\partial}{\partial y} c_{gy} N = \frac{S}{\sigma} \tag{11}$$

where the group celerity c_g is given, according to the linear wave theory, as

$$c_g = \frac{1}{2} c\left(1 + \frac{2kY}{\sinh(kY)}\right) \tag{12}$$

where c is the phase celerity ($c = \sigma/k$).

[35] Finally, it is important to note that the wave action conservation equation cannot reproduce diffraction. Because diffraction affects the wave field in a region of size equal to ~1–2 wavelengths behind an obstacle and because the wavelength inside the lagoon of Venice is far smaller than the grid size, diffraction can be neglected to a first approximation.

[36] Equation (11) is solved with an upwind finite volume scheme using the same mesh of the hydrodynamic model. The wind wave model computes the wave action in each element at each time step and, using the linear theory, the significant wave height.

[37] The term S on the right hand side of equation (11) describes all the external physical phenomena contributing to wave energy. They can be either positive e.g., wind energy input, or negative e.g., bottom friction, white capping, and depth-induced breaking. The implementation of each source term in the model is described in the following paragraphs.

3.1. Wind Generation

[38] A seminal discussion of wind wave generation was made by *Cavaleri and Malanotte-Rizzoli* [1981]. When considering the transfer of wind energy to waves two different mechanisms can be identified. The first one is the resonance phenomenon between free surface and turbulent pressure fluctuations. These fluctuations are due to the local wind field, and they move with the wind over the water surface. The corresponding energy growth is linear in time and expressed therefore by [*Phillips*, 1957]

$$\frac{\partial E}{\partial t} = \alpha \tag{13}$$

where α is a function of frequency and wind characteristics. Using the expression for the atmospheric turbulent pressure spectrum suggested by *Phillips* [1966] and based on the measurements of *Willmarth and Wooldridge* [1962] in a wind tunnel, the expression for α implemented in the model is

$$\alpha(k) = \frac{80\rho_a^2\sigma}{\rho_w^2 g^2 k^2} c_d^2 U^4 \tag{14}$$

where ρ_a is the air density, ρ_w is the water density, c_d = 0.001 is a drag coefficient, and U is the wind speed in m/s. It is easily seen that equation (13) describes energy transfer to the sea even when the initial condition is a flat free surface (i.e., from $E = 0$).

[39] Once the water surface is disturbed, it in turn disturbs the wind flow field over it, causing a greater transfer of energy from wind to waves. This results in a feedback mechanism leading to an exponential growth of the energy expressed by

$$\frac{\partial E}{\partial t} = \beta E \tag{15}$$

Barnett [1968] found a good fit between (15) and his experimental data through the use of

$$\beta(k) = 5\frac{\rho_a}{\rho_w} f\left(\frac{U\cos\delta}{c} - 0.90\right) \tag{16}$$

where f is the wave frequency ($f = 1/T$) and δ is the angle between wind and wave vector. Since the model assumes that waves and wind are aligned then $\delta = 0$ in the above equation. This second mechanism, as it can be deduced from equation (15), increases the wave energy only if some waves already exist.

[40] Equation (16) is obtained by a direct fit to experimental data [*Barnett and Wilkerson*, 1967]. We adopt this expression because it implicitly contains all information about the physical processes, such as nonlinear interactions [*Hasselmann et al.*, 1973; *Hasselmann*, 1974; *Snyder et al.*, 1978], which are not explicitly described in the present model.

[41] Combining (14) and (15), we obtain the total wind generation as

$$S_{wg} = \alpha + \beta E \tag{17}$$

3.2. Bottom Friction

[42] There are different mechanisms for wave energy dissipation at the bottom, such as energy dissipation through percolation, friction, motion of the soft muddy bottom, and bottom scattering. Bottom friction appears to be the most important mechanism for wave energy dissipation. The general expression for bottom friction can be written as

$$S_{bf} = -2C_f \frac{k}{\sinh(2kY)} E \tag{18}$$

where C_f is a dissipation coefficient, k is the wave number and Y is water depth.

[43] Different formulations can be found in the literature for the dissipation coefficient C_f. *Padilla-Hernàndez and Monbaliu* [2001] test four different expressions for wave energy dissipation by bottom friction. They conclude that the semiempirical formulation proposed by *Collins* [1972] gives very good results even when data are much different from those adopted by the author to derive his equation. Therefore the formulation given by *Collins* [1972] is implemented in the present model. Using the linear wave theory for bottom velocity, bottom friction is expressed as

$$S_{bf} = -4c\frac{\pi H}{T}\frac{k}{\sinh(kY)\sinh(2kY)} E \tag{19}$$

where H is the significant wave height, T is wave period and c a coefficient set equal to 0.015 after *Collins* [1972].

[44] If depth-induced breaking is present, equation (19) proposed by *Collins* [1972] is no longer applicable. In this case we assume that the most relevant dissipation process is wave breaking. For this reason the source term S_{bf} in the model is weighted by a factor complementary to the breaking probability Q_b (Q_b is detailed below) such that, in the presence of depth-induced breaking, the bottom friction term is minimized and does not produce any effect when breaking is certain ($Q_b = 1$).

3.3. White Capping

[45] White capping is a dissipative process related to wave breaking when the steepness limit of the wave is reached during propagation. There is a general agreement

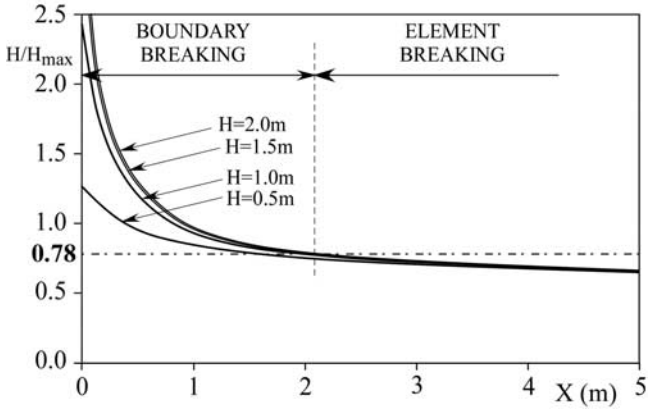

Figure 2. Spatial evolution of wave height after depth-induced breaking. We distinguish between boundary breaking and element breaking. The simulations refer to waves of different height, H that run into a shallower area 0.5 m deep, while propagating.

that white capping is the dominant dissipative mechanism at moderate and high wind speeds. Even though the physical meaning of white capping is intuitive, it is extremely difficult to model the process in detail. Models presented in the literature are of empirical derivation.

[46] The expression implemented in the present model is the one suggested by *Komen et al.* [1984] based on the previous work by *Hasselmann* [1974]:

$$S_{wc} = -c\sigma\left(\frac{\gamma}{\gamma_{PM}}\right)^{m} E \tag{20}$$

where γ is the integral wave steepness parameter, i.e., $\gamma = E\sigma^4/g^2$, σ is the relative frequency, $\gamma_{PM} = 4.57 \times 10^{-3}$ is the theoretical value of γ for a Pearson-Moskowitz spectrum, the exponent m is suggested by *Komen et al.* [1984] to equal 2. After some testing *Komen et al.* [1984] adopt for c the value that produces the best fit of the Pearson-Moskowitz spectrum ($c = 3.33 \times 10^{-5}$).

3.4. Depth-Induced Breaking

[47] The method suggested by *LeMéhauté* [1962] is here used to compute depth-induced breaking effects. In this approach the energy dissipation due to depth-induced breaking is computed as equivalent to that of a bore having the same height. Although the flow conditions on either sides of the breaking wave are not uniform, as required by the steady bore theory, the computed dissipation has the correct order of magnitude.

[48] To apply this scheme to irregular waves, *Battjes and Janssen* [1978] suggest a probabilistic approach for the breaking criterion which better embodies the physics of the process. They assume a Rayleigh-type probability distribution for the wave heights cut to the threshold $H_{max} = 0.78\ h$, where h is the water depth. Note that this threshold is the classic breaking criterion proposed by *McCowan* [1891].

[49] The expression for the breaking source term is then

$$S_{brk} = \frac{2\alpha}{T} Q_b \left(\frac{H_{max}}{H_{rms}}\right)^2 E \tag{21}$$

where Q_b is the probability that waves with height H_{rms} will break. The following implicit expression for Q_b was suggested by *Battjes and Janssen* [1978] and used in the present model

$$\frac{1 - Q_b}{\ln Q_b} = -\left(\frac{H_{rms}}{H_{max}}\right)^2 \tag{22}$$

where H_{rms} is the parameter of the Rayleigh-type distribution which is assumed to be equal to the wave height computed by the model in each grid element.

[50] In addition, for depth-induced wave breaking, we carry out an analysis similar to the analysis used to determine the characteristic decay time of the wave field. In this case we are interested in the space evolution of the wave energy due to the breaking dissipation process. Using (21), we numerically solve the equation $\partial N/\partial x = -S_{brk}$ in order to follow the evolution of wave energy (i.e., wave height) after a sharp variation in bottom elevation. Because the spatial scale considered is very small, all the other source terms are not considered in this analysis.

[51] Results of this analysis show that a large percentage of the global dissipation occurs in the very first meters after the discontinuity in bottom elevation (Figure 2). This suggests that the dissipation by breaking should be divided into two different parts. A first dissipation, hereafter referred to as "boundary breaking", occurs at the boundary between the deeper and the shallower element; whereas the second dissipation, the "element breaking", gradually develops in the downstream computational element.

[52] The boundary breaking process is implemented in the model through the comparison of wave energy which is potentially conveyed from the deeper to the shallower element and the maximum wave energy allowed for the shallower element. The latter is computed evaluating the wave energy ($E = \rho_w g H^2/8$) assuming the maximum wave height H equal to 0.78 times the water depth, following the *McCowan* [1891] breaking criterion. More precisely, if the energy conveyed between two adjoining elements is bigger than the maximum wave energy the model computes the energy flux using this maximum energy value. In this way we assume that the large dissipation occurring in the very first meters after the discontinuity in bottom elevation (Figure 3) is concentrated at the boundary between the elements.

[53] The element breaking is instead described in the standard way, i.e., by using the source term formulation (21). This division of the breaking process is physically based and makes the numerical scheme more stable and accurate.

[54] The above approach makes it possible to separate the amount of energy locally dissipated because of a sudden variation of bathymetry from the continuously occurring dissipation over horizontal or gently sloping bottom surfaces (Figure 3). Moreover, distinguishing the energy dissipation due to breaking at topography discontinuities has a potential use in assessing morphologic evolution of tidal marsh edges [*Allen*, 2000].

4. Model Validation

[55] The hydrodynamic model is described and validated elsewhere [*Defina et al.*, 1994; *D'Alpaos and Defina*, 1995;

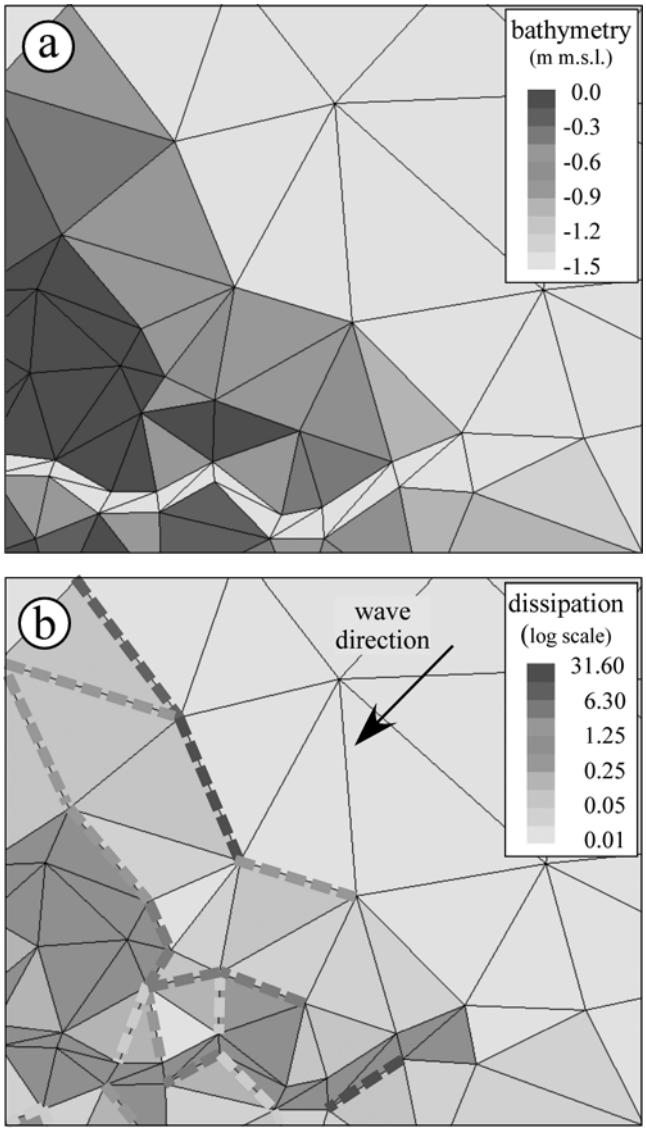

Figure 3. Spatial distribution of energy dissipation produced by depth-induced breaking. (a) Bathymetry of the studied area; (b) energy dissipation due to ''boundary breaking'' and ''element breaking.'' The dissipation by boundary breaking is shown as a dotted line with the gray scale proportional to the dissipation.

Defina, 2000]. Here we present additional model validations focusing on the importance of the wind action on the free surface displacement. All simulations are performed using a refined mesh reproducing the actual topography of the Venice lagoon comprising 35,000 nodes and 67,000 elements (Figure 4).

[56] Recent measurements of wind speed, direction, and wave heights are provided by the Ministero delle Infrastrutture e dei Trasporti, Magistrato alle Acque di Venezia, through Consorzio Venezia Nuova. These field measurements are taken at two different stations: the first (1BF) is on a shoal in the northern part of the lagoon (San Felice marsh) and the second (2BF) is in a deeper area in the southern part of the lagoon (Fondo dei Sette Morti; see Figure 5).

[57] Available data at these stations consist of synchronous wave and wind measurements collected over a ten minutes period. The data used for this study include the significant wave height, the averaged wind speed and direction, and the water level at the station.

[58] Other stations inside the lagoon of Venice collect tidal elevation data only. The city of Venice kindly provided us records from five of these stations located respectively at the three inlets (Lido, Malamocco, and Chioggia Inlets), at the Chioggia station in the southern part of the lagoon, and at the Saline station in the northern part of the lagoon (see Figure 5).

[59] Data collected at the 1BF and 2BF stations also provide information on local meteorological conditions. The first simulation we perform reproduces a weather condition characterized by no wind during 2–5 March 2003. Water levels at the three inlets, imposed in the hydrodynamic model as boundary conditions, are shown in Figure 6a. Computed water levels at the Saline, Chioggia, 1BF and 2BF stations compare favorably with field data (Figures 6b and 6c).

[60] The second simulation reproduces a windy period (3 April 2003) characterized by Bora wind blowing from northeast with a speed in the range between 12 and 16 m/s (Figure 7a). Bora wind affects near-coast sea levels resulting in lower elevations at the Lido inlet than at the Chioggia inlet (Figure 7b). Wind setup strongly affects the hydrodynamics within the lagoon. This is shown in Figure 7c and 7d where the measured water levels at 1BF and 2BF are compared with the water levels computed by the hydrodynamic model with and without wind shear stresses.

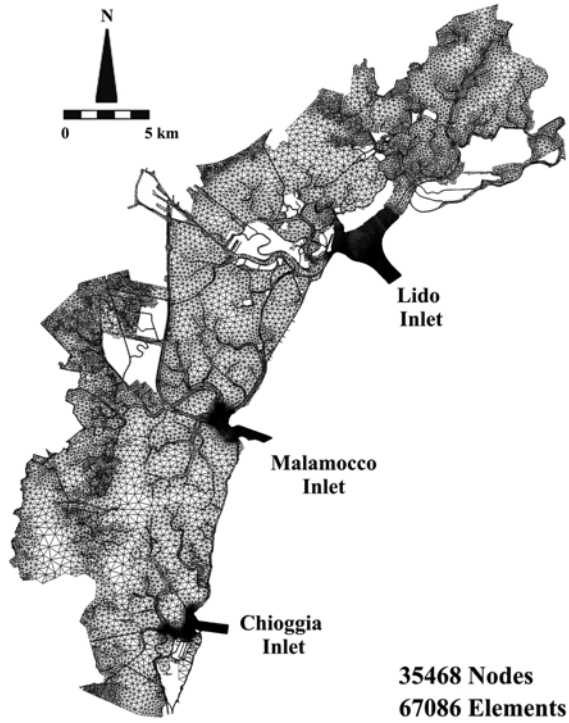

Figure 4. Mesh reproducing the lagoon of Venice used in the simulations (35,000 nodes and 67,000 elements).

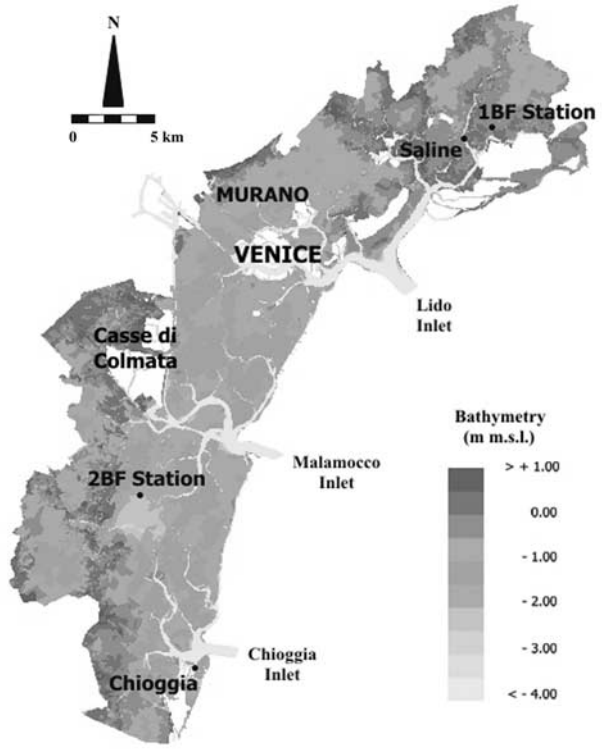

Figure 5. Bathymetry of the Venice lagoon with the locations of the two stations where wind and waves data were collected. Station 1BF, north lagoon, "barena San Felice"; station 2BF, south lagoon, "fondo dei Sette Morti." Chioggia and Saline are other two stations where only water level data are continuously collected.

[61] The neglecting of wind shear stresses produces results that do not fit the measured water level at the two stations, with higher levels at the northern 1BF station and lower levels at the southern 2BF station. The wind setup, evident in the simulation with wind shear stresses, leads to a reduction of tidal levels leeward and an increase windward, in agreement with the data.

[62] The hydrodynamic importance of the wind shear stress on the free surface inside the lagoon of Venice is even more evident when the water discharges at the three inlets are considered. When considering wind shear stress effects, simulated discharges at the Lido inlet, increase during flood and decrease during ebb (Figure 8a). The opposite trend is experienced at the Chioggia inlet (Figure 8c), while no substantial change occurs at the Malamocco inlet (Figure 8b). Globally, wind setup during Bora conditions produces a residual current flowing from the Lido inlet toward the Chioggia inlet.

[63] We then perform a set of simulations to validate the wind wave model by reproducing the wind wave field inside the lagoon of Venice during different meteorological conditions. In a first set of simulations hydrodynamic effects related to tidal oscillations are not considered. Therefore only initial conditions of uniform level all over the lagoon are introduced without any hydrodynamic boundary condition. During the simulations the initial water level changes only because of the drag effect of the wind on the water surface.

[64] In these simulations the model is constrained by different wind speeds and directions, always starting from a uniform water level in the lagoon (see Tables 1–6). The simulations are stopped when the equilibrium condition for wind waves is reached.

[65] The simulations match groups of data in which the wind is blowing long enough (at least an hour) in the same direction and at the same speed so that the recorded wave field can be considered as stable. Results are summarized in Tables 1–6, with the model results reported in the last row, showing a good agreement between the model and the field data.

[66] To give a more complete validation of the model results and to assess the importance of the coupling between tidal currents and wind waves, we perform two additional simulations forcing the model simultaneously with real hydrodynamic boundary conditions at the three inlets and assuming a real wind field blowing on the lagoon. The two

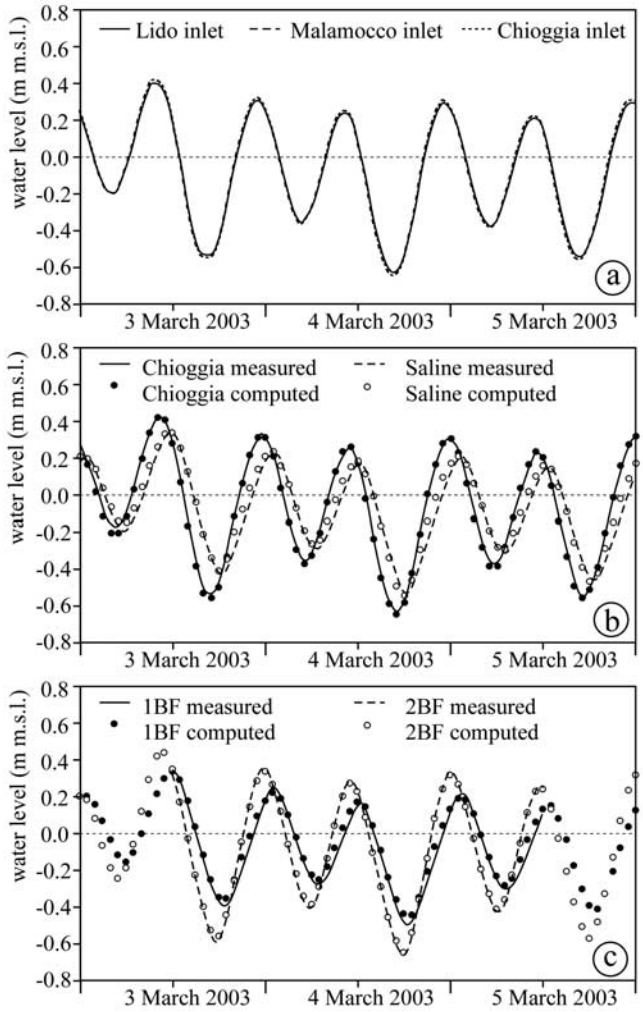

Figure 6. For 2–3 March 2003. (a) Measured water levels at the three inlets (Lido, Malamocco, and Chioggia); (b) comparison of measured (solid and dashed lines) and computed (circles) water levels at Chioggia and Saline stations; (c) comparison of the measured (solid and dashed lines) and computed (circles) water levels at stations 1BF and 2BF.

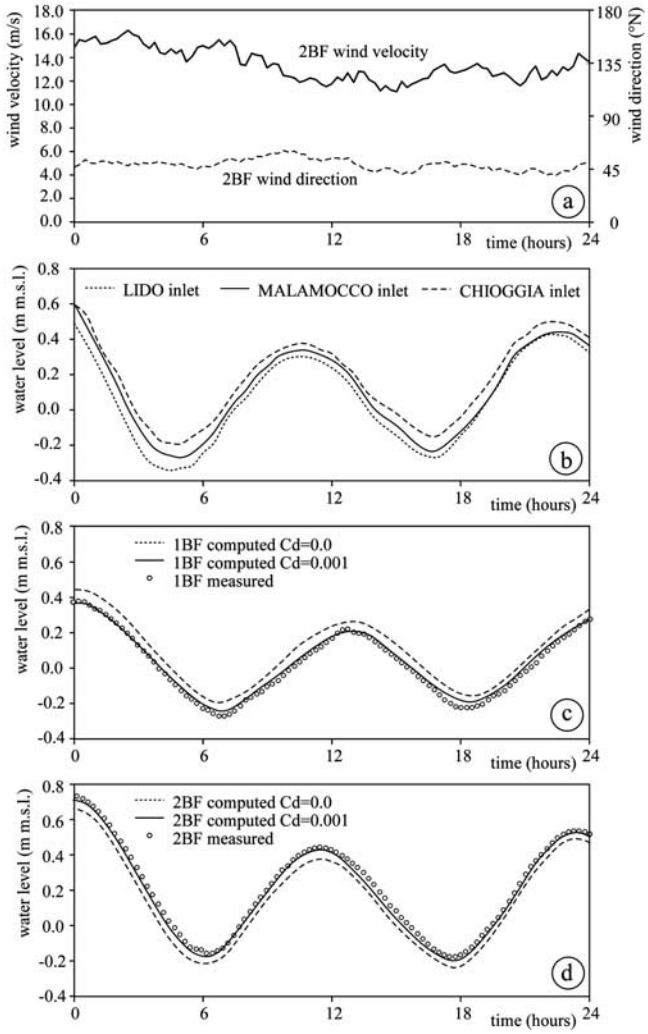

Figure 7. For 3 April 2003. (a) Measured wind velocity (solid line) and direction (dashed line) above the Venice lagoon; (b) measured water levels at the three inlets (Lido, Malamocco, and Chioggia); comparison of measured (solid lines) and computed water levels at stations (c) 1BF and (d) 2BF without wind shear stress at the free surface (dashed lines) and with a drag coefficient for the wind shear stress equal to 0.001 (circles).

periods of time reproduced by the model are 3 April 2003 and 16–17 February 2003. To define the wind field forcing the model, data collected at the 2BF station are used (a comparison with the wind speed and direction collected at 1BF proves that the wind field can be consider uniform above the entire lagoon).

[67] On 3 April 2003 a Bora wind was blowing from 45°N with a speed ranging from 12 to 16 m/s (see Figure 7a). The second period reproduced is, instead, characterized by a wind blowing from 60°N with an averaged speed ranging between 10 and 12 m/s.

[68] Figure 9 reproduces two diagrams comparing the significant wave height measured at 1BF and 2BF station with the wave height evaluated by the model. The agreement for both periods (Figures 9a and 9b) is quite good. By looking at the results it is evident that a sinusoidal-like variation of significant wave height follows the tidal oscillation, thus confirming the influence of water level on wave height and the strong coupling between wind waves and hydrodynamics.

[69] An example of the reproduced wave field inside the lagoon of Venice is given in Figure 10. Figure 10 refers to the 16–17 February 2003 simulation forced by a wind blowing from 60°N. Two different instants are reproduced referring respectively to a very low tide (Figure 10a) and to a high tide (Figure 10b). Again, it is clear the influence of water level on wave field in a very shallow basin like the Venice lagoon. As it can be noticed, the model effectively reproduces the sheltering effect of islands, with reduced wave height on the downwind side.

5. Wind Waves Effect on Bottom Shear Stresses

[70] A first application of the model shows the complementary effects of tidal currents and wind waves on bottom

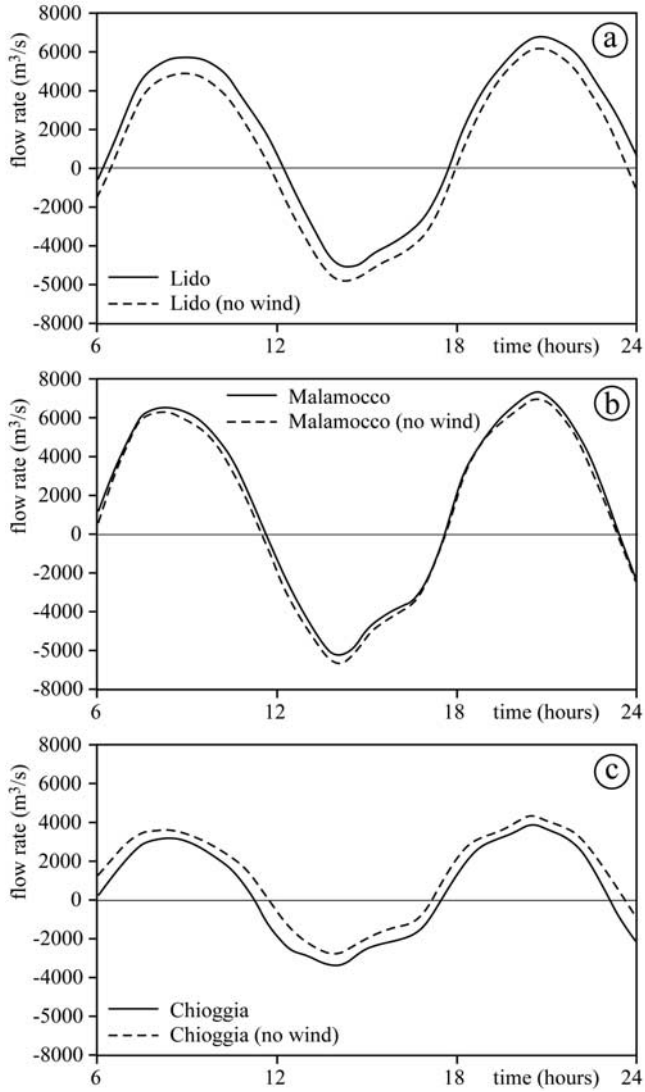

Figure 8. For 3 April 2003. Computed water discharges at the three inlets, (a) Lido, (b) Malamocco, and (c) Chioggia, neglecting the wind shear stress at the free surface (dashed lines) and considering a drag coefficient for the shear stress at the free surface equal to 0.001 (solid lines).

Table 1. Station 2BF[a]

2 April 2003, LT	H_{mo}, m	T_s, s	U_{wind}, m/s	Direction, °N	h_w, m
1500	0.51	2.06	10.57	48	0.13
1515	0.51	2.11	10.63	47	0.10
1530	0.51	1.97	10.41	48	0.07
1545	0.50	1.97	10.82	48	0.04
1600	0.48	1.98	10.57	49	0.01
Model[b]	0.54	2.00	10.00	45	0.06

[a]Bora Wind (45°N) blowing at 10 m/s over an initial water level equal to 0.00 m above mean sea level (amsl).
[b]Model results.

Table 3. Station 2BF[a]

6 April 2003, LT	H_{mo}, m	T_s, s	U_{wind}, m/s	Direction, °N	h_w, m
0900	0.36	1.76	8.50	126	0.15
09.15	0.41	1.87	8.64	129	0.19
0930	0.45	1.91	8.97	131	0.24
0945	0.47	1.92	8.83	126	0.28
1000	0.44	1.94	8.48	129	0.32
1015	0.45	1.85	8.09	128	0.36
1030	0.41	1.86	7.89	133	0.40
Model	0.50	2.00	8.00	135	0.50

[a]Sirocco Wind (135°N) blowing at 8 m/s over an initial water level equal to 0.50 m amsl.

shear stresses. In the model we evaluate the bottom shear stress indicating the resuspension capacity of tidal currents and wind waves during different simulations.

[71] When discussing sediment resuspension, it is very important to consider bottom sediment characteristics, since the behavior of cohesive sediments is very different from loose sediments. The composition of bottom sediments substantially varies within the lagoon of Venice. At the three inlets and in the large channels the bottom is almost completely composed of fine sand, but in the tidal flats and in the marshes it is common to find silt and up to 5–10% of clay [*Cola and Simonini*, 2002].

[72] *Amos et al.* [2004] studied the stability of tidal flats in the Venice lagoon collecting in situ measurements using two benthic, annular flumes (Sea Carousel and Mini Flume). They simultaneously deployed the two instruments at 24 sites in August 1998. Of these sites, 13 were reoccupied during February 1999. The sites were considered representative of the range in bed/habitat types for the Venice lagoon. All sites are on cohesive clayey silt with exception of three sites, close to the Lido and Malamocco inlets, which are sandy and colonized by seagrass. Sea Carousel and Mini Flume results showed similar overall trends in mean erosion thresholds. The lagoon-averaged summer values of the critical shear stress (τ_{cr}) were 1.10 and 0.82 Pa, respectively, whereas during winter, they were 0.69 and 0.74 Pa.

[73] In this paper we focus on the coupled influence of wind waves and tidal currents on bottom shear stresses and potential for erosion. Sediment transport processes are beyond the aim of this study and will be the subject of future research.

[74] Both tidal currents and wind waves contribute to the production of bottom shear stresses in the lagoon. To evaluate the tidal current contribution ($\tau_{b,\mathrm{curr}}$), we substitute the value of the current velocity in equation (6).

Table 2. Station 2BF[a]

2 April 2003, LT	H_{mo}, m	T_s, s	U_{wind}, m/s	Direction, °N	h_w, m
2045	0.79	2.24	15.74	39	0.51
2100	0.80	2.34	14.50	39	0.55
2115	0.75	2.30	15.23	41	0.59
2130	0.81	2.35	16.16	43	0.63
2145	0.76	2.36	14.43	43	0.67
2200	0.73	2.40	16.05	42	0.71
2215	0.73	2.49	14.59	44	0.73
Model	0.62	2.00	15.00	45	0.64

[a]Bora Wind (45°N) blowing at 15 m/s over an initial water level equal to 0.50 m amsl.

[75] For the waves contribution ($\tau_{b,\mathrm{wave}}$) we use

$$\tau_{b,\mathrm{wave}} = \frac{1}{2} f_w \rho_w u_m^2 \tag{23}$$

where u_m is the maximum horizontal orbital velocity associated with the wave propagation and f_w is the wave friction factor. The bottom velocity u_m, following the linear theory, can be evaluated by

$$u_m = \frac{\pi H_w}{T \sinh(kh)} \tag{24}$$

where H_w is the wave height, T is the wave period, k is the wave number, and h is the water depth.

[76] The wave friction factor can be approximated as [*Soulsby*, 1997]

$$f_w = 1.39 \left[\frac{u_m T}{2\pi (D_{50}/12)} \right]^{-0.52} \tag{25}$$

where D_{50} is the median grain diameter assumed equal to 20 μm according to the measurements of *Amos et al.* [2004] and *Cola and Simonini* [2002].

[77] Actual bed shear stress under the combined action of waves and currents is enhanced beyond the sum of the two contributions. This occurs because of the nonlinear interaction between the wave and current boundary layers. In the present model the empirical formulation suggested by *Soulsby*, [1995, 1997] is adopted. Accordingly, the mean bed shear stress τ_m is

$$\tau_m = \tau_{b,\mathrm{curr}} \left[1 + 1.2 \left(\frac{\tau_{b,\mathrm{wave}}}{\tau_{b,\mathrm{curr}} + \tau_{b,\mathrm{wave}}} \right)^{3.2} \right] \tag{26}$$

[78] The maximum shear stress ($\tau_{\max}$), due to the combined action of waves and currents is given as a vector

Table 4. Station 1BF[a]

2 April 2003, LT	H_{mo}, m	T_s, s	U_{wind}, m/s	Direction, °N	h_w, m
1500	0.19	1.38	11.17	35	0.82
1515	0.19	1.31	11.26	37	0.78
1530	0.18	1.38	10.90	39	0.75
1545	0.18	1.40	10.50	41	0.72
1600	0.19	1.29	9.83	35	0.70
Model	0.24	2.00	10.00	45	0.69

[a]Bora Wind (45°N) blowing at 10 m/s over an initial water level equal to 0.50 m amsl.

Table 5. Station 1BF[a]

30 April 2003, LT	H_{mo}, m	T_s, s	U_{wind}, m/s	Direction, °N	h_w, m
0445	0.03	-	3.67	111	0.41
0500	0.04	-	4.65	123	0.38
0515	0.04	1.75	4.35	123	0.37
0530	0.04	1.35	4.20	122	0.36
0545	0.03	1.84	3.56	129	0.36
Model	0.00	2.00	5.00	135	0.50

[a]Scirocco Wind (135°N) blowing at 5 m/s over an initial water level equal to 0.00 m amsl. Dash indicates data absent.

addition of τ_m and shear stress induced by waves [*Soulsby*, 1997] i.e.,

$$\tau_{max} = \left[\left(\tau_m + \tau_{b,wave}\cos\phi\right)^2 + \left(\tau_{b,wave}\sin\phi\right)^2\right]^{1//2} \quad (27)$$

where ϕ is the angle between the current and the wave directions. Since maximum shear stress τ_{max}, rather than average stress τ_m, is responsible for the bottom sediments mobilization, all the results presented and discussed herein refer to the maximum total bottom shear stress.

[79] Figure 11 shows the spatial distribution of bottom shear stress computed with the model inside the lagoon of Venice at four different instants during 16–17 February 2003. Figure 11 shows a very low tide slack water condition (Figure 11a) at 1700 LT on 16 February 2003, a high tidal current condition (Figure 11b) at 2000 LT on 16 February 2003, a high tide slack water condition (Figure 11c) at midnight, and a second low tide slack water (Figure 11d) at 0400 LT on 17 February 2003. Figure 11 shows the tidal level at the Lido inlet. The wind field above the lagoon is characterized by a ~10–12 m/s wind blowing from approximately 60°N. High shear stress values are recognizable in the large channels departing from the three inlets only during ebb and flood (Figure 11b), while it is completely absent during times of high water slack and low water slack. Shear stress intensity and spatial distribution are extremely sensitive to water level inside the lagoon (see, e.g., Figure 11a and 11c). We note that the maximum shear stress on the tidal flats occurs for an average depth (see Figures 11a, 11b, and 11c), since in shallow water depths the wind stresses are unable to develop high waves, and in deep-water depths the bottom is too far from the surface to experience consistent shear stresses.

[80] Figure 12 shows the time evolution of the bottom shear stress at three different sites within the lagoon. The sites are chosen in a large channel close to the Lido inlet (Figure 12a), on a tidal flat close to the Murano island (Figure 12b), and on a tidal flat next to the Casse di Colmata (Figure 12c). The location of these sites is shown in Figure 11c. The bottom shear stress is evaluated by the model during a storm event measured on 16–17 February 2003. Each plot compares model results obtained with three different simulations, i.e., (1) without wind waves and without wind shear stresses; (2) with wind shear stresses; and (3) with both wind waves and wind shear stresses. Simulation results show that in deep channels wind waves negligibly affect bottom shear stresses, whereas there is a clear influence of wind stresses at the surface. On tidal flats, instead, bottom shear stresses are strongly enhanced when wind waves are included in the model (Figures 12b and 12c). Also wind stresses at the surface are important, affecting the bottom shear stresses produced by tidal currents. This is because wind stresses are responsible for a residual circulation in the lagoon that moves large volumes of water.

[81] It is worth noting that because of the presence of waves, bottom shear stresses exceed the critical value τ_{cr} for sediment erosion on tidal flats. On the contrary the bottom shear stresses are always smaller than the critical value when wind waves are not accounted in the model.

[82] This result is supported by Figure 13 mapping the regions where the bottom shear stress is greater than 0.7 Pa, i.e., the critical shear stress value for winter [*Amos et al.*, 2004]. No resuspension is possible on tidal flats and salt marshes if wind waves are not considered.

[83] Figure 13 further confirms that wind wave resuspension is complementary to tidal current resuspension since waves are able to produce shear stresses higher than the critical stress in shallower areas. The shear stress due to tidal currents is high only inside the large and deep

Table 6. Station 1BF[a]

2 April 2003, LT	H_{mo}, m	T_s, s	U_{wind}, m/s	Direction, °N	h_w, m
2045	0.45	1.70	15.53	23	0.91
2100	0.49	1.72	15.83	25	0.93
2115	0.53	1.63	16.34	25	0.94
2130	0.47	1.80	15.61	22	0.96
2145	0.44	1.69	14.70	22	0.95
2200	0.44	1.66	15.11	22	0.97
2215	0.44	1.68	14.59	22	0.97
Model	0.42	2.00	15.00	20	0.97

[a]Wind blowing from 20°N at 15 m/s over an initial water level equal to 1.20 m amsl.

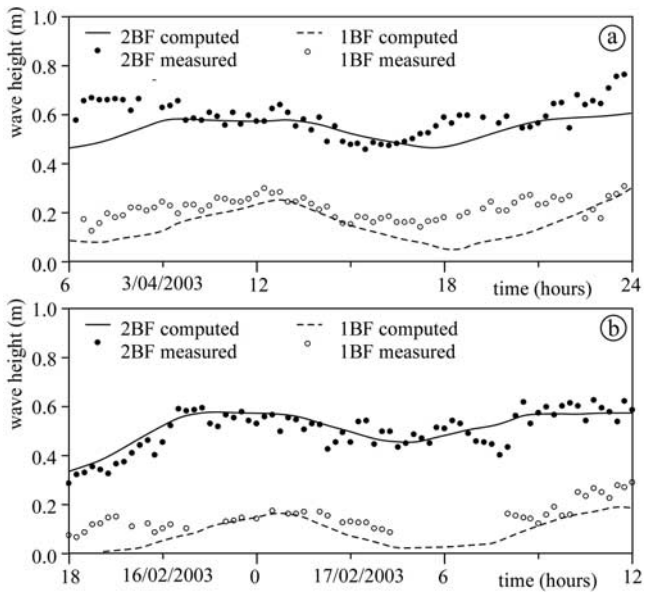

Figure 9. Comparison of measured (solid and dashed lines) and computed (circles) wave height at stations 1BF and 2BF during (a) 3 April 2003 and (b) 16–17 February 2003.

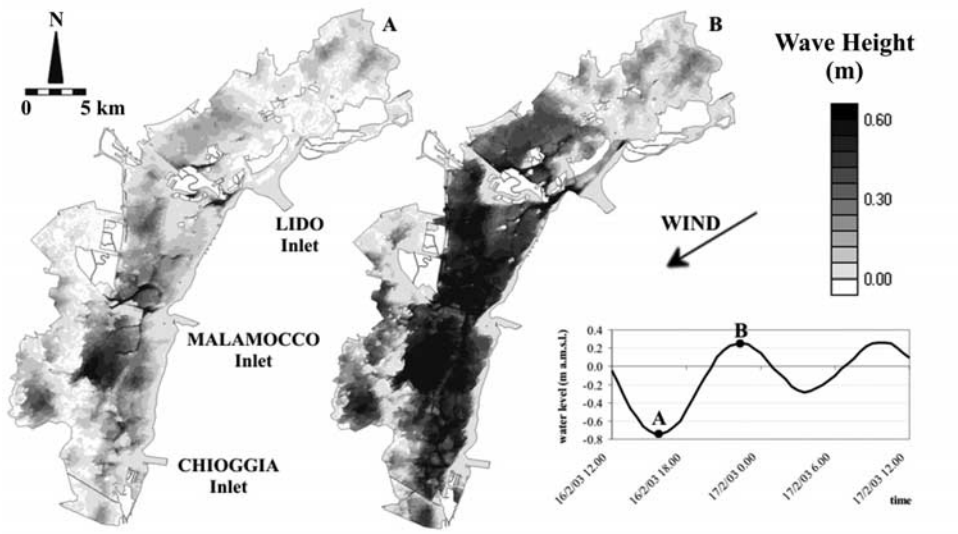

Figure 10. For 16–17 February 2003: spatial distribution of wave height evaluated by the model inside the Venice lagoon during tide propagation for (a) a very low tide and (b) a high.

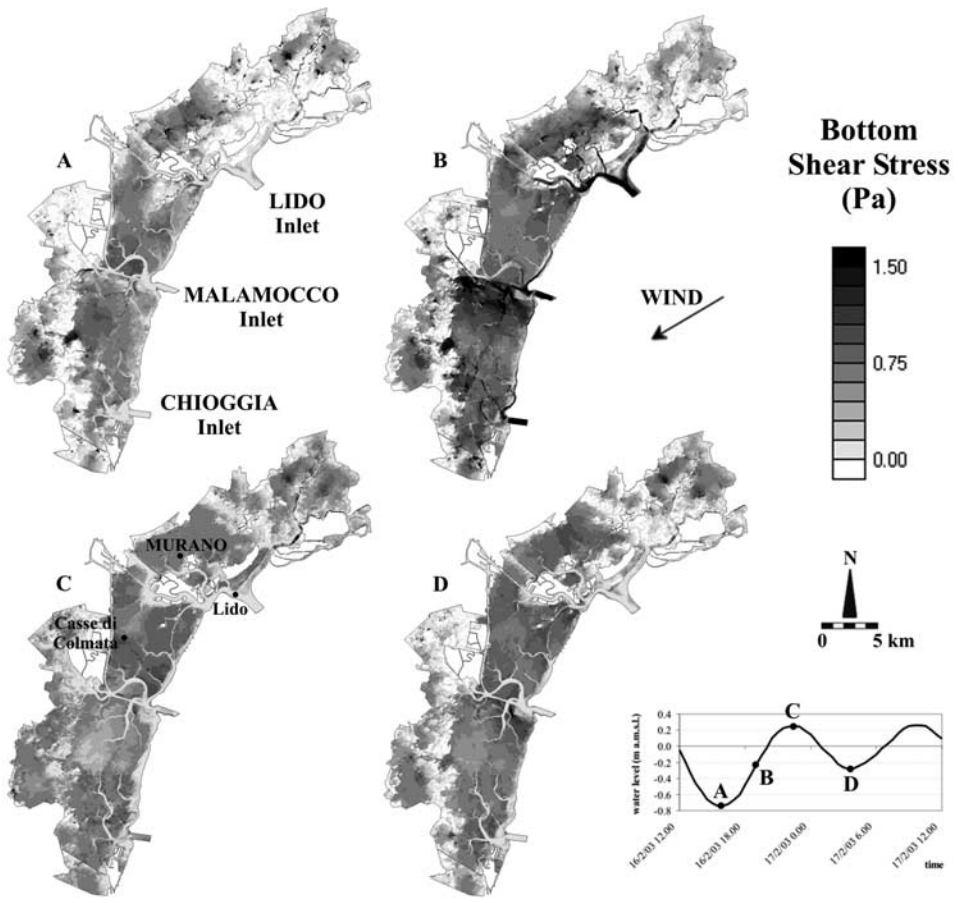

Figure 11. For 16–17 February 2003. Spatial distribution of bottom shear stress evaluated by the model inside the Venice lagoon during tide propagation for (a) a very low tide slack water condition, (b) a high tidal current flow condition, (c) a high tide slack water condition, and (d) a second low tide slack water condition.

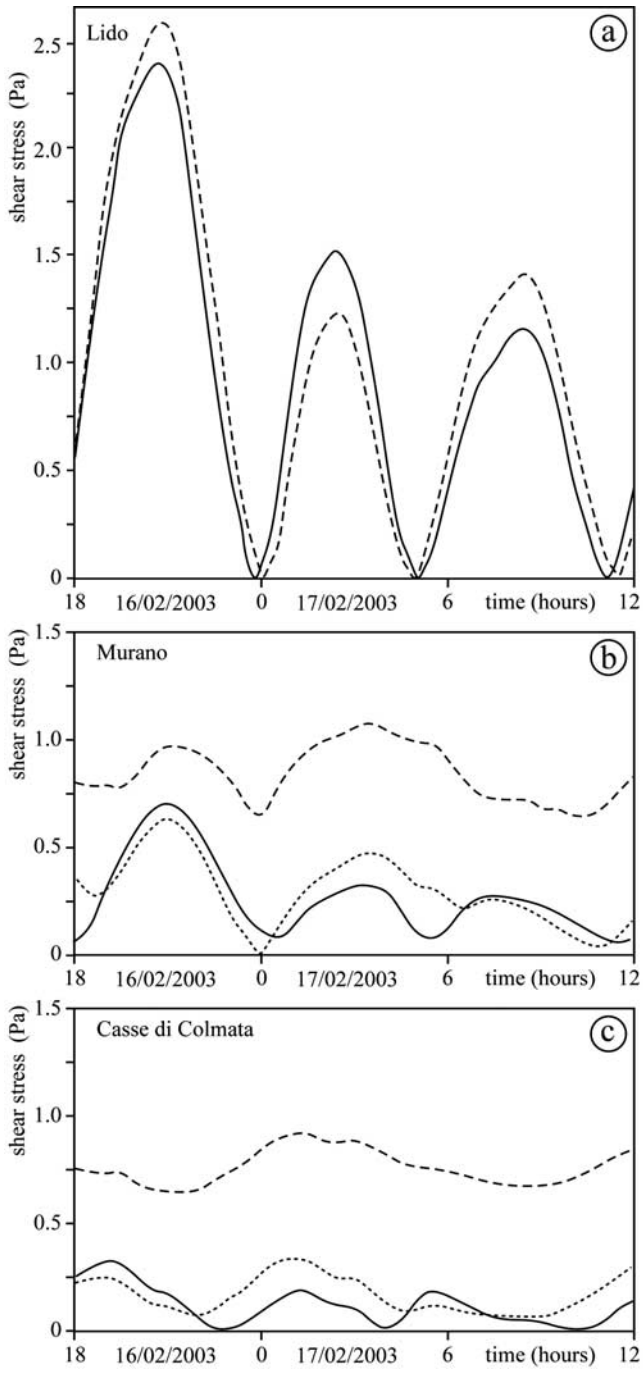

Figure 12. For 16–17 February 2003. Comparison of the shear stress at the bottom produced by the combined effect of wind waves and tidal currents (dashed), by tidal currents alone (dotted), and by tidal currents neglecting the wind shear stress at the free surface (solid). The comparison refers to (a) the Lido Inlet, (b) a tidal flat close to Murano Island, and (c) a tidal flat close to "Casse di Colmata."

channels, where most of the tidal flow is concentrated [*Fagherazzi and Furbish*, 2001; *Fagherazzi et al.*, 2003].

6. Conclusions

[84] A model describing the generation and propagation of wind waves inside a tidal basin is presented which solves the wave action conservation equation using a finite volume scheme. The wave model is coupled with a hydrodynamic model that uses the same domain discretization, thus optimizing the transfer of data between the tidal and the wave components. The model is utilized to map bottom shear stresses in the Venice lagoon under different tidal and wind conditions. The major conclusions of this study are listed below:

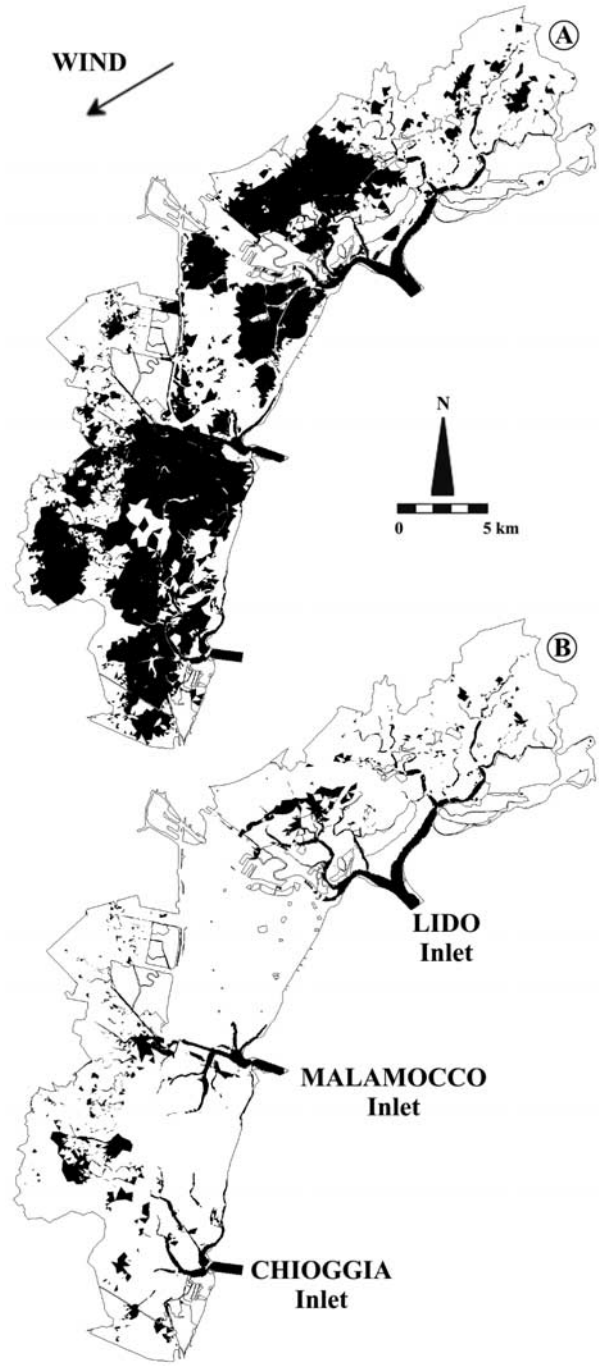

Figure 13. For 16 February 2003 at 2200 LT. Spatial distribution of the area experiencing a bottom shear stress greater than 0.7 Pa inside the Venice lagoon. Comparison of (a) simultaneous effect of tidal currents and wind waves and (b) the effect of tidal currents alone.

[85] 1. An undisputed advantage of the model resides in the finite element discretization that is more suitable to represent shallow tidal basins where deep and branched channels dissect tidal flats and salt marshes.

[86] 2. To realistically simulate the wave breaking at the banks of the major channels or at the marsh edges, the dissipation of wave energy is split in a boundary component that accounts for the breaking of waves in the first couple of meters of the bank and a uniform dissipation within the computational element.

[87] 3. The feedbacks between wind waves and tidal hydrodynamics are of paramount importance in shallow basins. Wind shear stresses modify tidal hydrodynamics by introducing residual circulations whereas the tidal elevation is modulating the wave height within the basin. Both tidal hydrodynamics and wind waves are affecting the bottom shear stresses responsible for sediment erosion and resuspension.

[88] 4. In deep channels the maximum bottom shear stress occurs during flood and ebb conditions, i.e., when tidal currents are peaking. Shear stresses caused by wind waves are negligible whereas wind stresses at the water surface have a remarkable influence on bottom stresses.

[89] 5. On tidal flats wind waves considerably increase bottom shear stresses. The maximum shear stress caused by wind waves occurs for an average depth on the tidal flat, since in shallow water depths the wind stresses are unable to develop high waves, and in deep-water depths the bottom is too far from the surface to experience consistent shear stresses. Wind stresses at the water surface clearly affect bottom shear stresses by producing residual currents that increase the local velocity on the tidal flats.

[90] 6. Comparison between the distribution of bottom shear stresses and the critical shear stress for erosion in the lagoon clearly shows that without the effect of wind waves the bottom sediments cannot be resuspended on tidal flats.

[91] **Acknowledgments.** This research has been funded by Consorzio per la Gestione del Centro di Coordinamento delle Attività di Ricerca inerenti il Sistema Lagunare di Venezia (Co.Ri.La.) under the research program "Modellazione matematica e fisica di alcuni processi di sedimentazione nella Laguna di Venezia" (linea 3.14); by Comune di Venezia, Co.Ri.La., "Modificazioni morfologiche della laguna, perdita e reintroduzione dei sedimenti"; by the Office of Naval Research, award N00014-05-1-0071; and by the Center for Earth Surface Processes Research (CESPR), Florida State University. The authors wish to thank the Ministero delle Infrastrutture e dei Trasporti, Magistrato alle Acque di Venezia, through its concessionary Consorzio Venezia Nuova for the field data essential to validate the model. Luca Carniello wants to thank Paolo Martini and Meg Streepey for their helpful and detailed review of this paper.

References

Allen, J. R. L. (2000), Morphodynamics of Holocene saltmarshes: A review sketch from the Atlantic and southern North Sea coasts of Europe, *Quat. Sci. Rev.*, *19*, 1151–1231.

Amos, C. L., A. Bergamasco, G. Umgiesser, S. Cappucci, D. Cloutier, L. DeNat, M. Flindt, M. Bonardi, and S. Cristante (2004), The stability of tidal flats in Venice lagoon—The results of in-situ measurements using two benthic, annular flumes, *J. Mar. Syst.*, *51*, 211–241.

Barnett, T. P. (1968), On the generation, dissipation and prediction of ocean wind waves, *J. Geophys. Res.*, *73*, 513–529.

Barnett, T. P., and J. C. Wilkerson (1967), On the generation of wind waves as inferred from airbone measurements of fetch-limited spectra, *J. Mar. Res.*, *25*, 292–321.

Battjes, J. A., and J. P. F. M. Janssen (1978), Energy loss and set-up due to breaking of random waves, in *Proceedings of 16th International Conference on Coastal Engineering*, pp. 569–587, Am. Soc. of Civ. Eng., New York.

Bettenetti, A., F. Mattarolo, and P. Silva (1995), Reconstruction of saltmarshes in the Venice lagoon, in *Proceedings of the 2nd International Conference on the Mediterranean Coastal Environment (MEDCOAST 95), October 24–27 1995, Tarragona, Spain*, edited by E. Ozhan, pp. 921–935, MEDCOAST Secr., Middle East Tech. Univ., Ankara, Turkey.

Booij, N., R. C. Ris, and L. H. Holthuijsen (1999), A third-generation wave model for coastal regions: 1. Model description and validation, *J. Geophys. Res.*, *104*, 7649–7666.

Cavaleri, L., and P. Malanotte-Rizzoli (1981), Wind wave prediction in shallow water, *J. Geophys. Res.*, *86*, 961–973.

Cola, S., and P. Simonini (2002), Primi risultati di misure di pressione neutrale nei terreni delle barene della Laguna di Venezia, paper presented at First Annual Workshop of Corila Research Program 2002–2004, Co.Ri.La., Venice, Italy.

Collins, J. I. (1972), Prediction of shallow water spectra, *J. Geophys. Res.*, *77*, 2693–2707.

D'Alpaos, L., and A. Defina (1995), Modellazione matematica del comportamento idrodinamico di zone a barena solcate da una rete di canali minori, Estratto da Rapp. e Studi, Ist. Veneto di Sci., Lett. ed Arti, Venice, Italy.

D'Alpaos, L., and P. Martini (2003), The influence of inlet configuration on sediment loss in the Venice lagoon, paper presented at Flooding and Environmental Challenges for Venice and Its Lagoon: State of Knowledge 2003, Churchill Coll., Cambridge, U.K., 14–17 Sept.

Day, J. W., J. Rybczyk, F. Scarton, A. Rismondo, D. Are, and G. Cecconi (1999), Soil accretionary dynamics, sea-level rise and the survival of wetlands in Venice lagoon: A field and modelling approach, *Estuarine Coastal Shelf Sci.*, *49*(5), 607–628.

Defina, A. (2000), Two-dimensional shallow water equations for partially dry areas, *Water Resour. Res.*, *36*, 3251–3264.

Defina, A. (2003), Numerical experiments on bar growth, *Water Resour. Res.*, *39*(4), 1092, doi:10.1029/2002WR001455.

Defina, A., L. D'Alpaos, and B. Matticchio (1994), A new set of equations for very shallow water and partially dry areas suitable to 2D numerical models, in *Proceedings of the Specialty Conference on Modelling of Flood Propagation Over Initially Dry Areas, Milan (Italy) 29 June–1 July 1994*, edited by P. Molinaro and L. Natale, pp. 72–81, Am. Soc. of Civ. Eng., New York.

Dingemans, M. W. (1997), *Water Wave Propagation Over Uneven Bottoms*, part 1, *Linear Wave Propagation*, *Adv. Ser. Ocean Eng.*, vol. 13, 471 pp., World Sci., River Edge, N. J.

Donelan, M. A. (1977), A simple numerical model for wave and wind stress prediction, report, Natl. Water Res. Inst., Burlington, Ont., Canada.

Fagherazzi, S., and D. J. Furbish (2001), On the shape and widening of salt marsh creeks, *J. Geophys. Res.*, *106*, 991–1005.

Fagherazzi, S., A. Bortoluzzi, W. E. Dietrich, A. Adami, S. Lanzoni, M. Marani, and A. Rinaldo (1999), Tidal networks: 1. Automatic network extraction and preliminary scaling features from digital elevation maps, *Water Resour. Res.*, *35*(12), 3891–3904.

Fagherazzi, S., P. L. Wiberg, and A. D. Howard (2003), Tidal flow field in a small basin, *J. Geophys. Res.*, *108*(C3), 3071, doi:10.1029/2002JC001340.

Feola, A. (2002), Indagine numerica e sperimentale sui fenomeni di moto ondoso da vento in bassi fondali a batimetria irregolare, M.S. thesis, Dep. of Hydraul., Maritime, Environ. and Geotec. Eng., Univ. of Padua, Padua, Italy.

Gelci, R., H. Calazé, and J. Vassal (1956), Utilization des diagrammes de propagation à la prévision énergétique de la houle, *Inf. Bull. 8* (4), 160–197, Com. Cent. d'Océanogr. et d'Etudes des Côtes, Paris.

Hasselmann, K. (1974), On the spectral dissipation of ocean waves due to white-capping, *Boundary Layer Meteorol.*, *6*(1–2), 107–127.

Hasselmann, K., et al. (1973), Measurements of wind-wave growth and swell decay during the Joint North Sea Wave Project (JONSWAP), *Dtsch. Hydrogr. Zeit. Suppl.*, *12*(A8), 1–95.

Holthuijsen, L. H., N. Booij, and W. D. Grant (1989), A prediction model for stationary, short-crested waves in shallow water with ambient currents, *Coastal Eng.*, *13*, 23–54.

Komen, G. J., S. Hasselmann, and K. Hasselmann (1984), On the existence of a fully developed wind-sea spectrum, *J. Phys. Oceanogr.*, *14*, 1271–1285.

Leenknecht, D. A., A. Szuwalski, and A. R. Sherlock (1992), Automated coastal engineering system, Coastal Eng. Res. Center, U.S. Army Eng. Waterways Exp. Stn., Vicksburg, Miss.

LeMéhauté, B. (1962), On non-saturated breakers and the wave run-up, paper presented at the 8th International Conference on Coastal Engineering, Am. Soc. of Civ. Eng., Mexico City.

Lin, W., L. P. Sanford, B. J. Alleva, and D. J. Schwab (1998), Surface wind wave modeling in Chesapeake Bay, paper presented at the Third International Conference on Ocean Wave Measurements and Analysis, Am. Soc. of Civ. Eng., Virginia Beach, Va.

Lin, W., L. P. Sanford, B. J. Alleva, and S. E. Suttles (2002), Wave measurements and modeling in Chesapeake Bay, *Cont. Shelf Res.*, *22*, 2673–2686.

Martini, P., L. D'Alpaos, and L. Carniello (2003), Un modello matematico bidimensionale per lo studio dell'idrodinamica e del trasporto di sedimenti nella Laguna di Venezia, paper presented at the Second Annual Workshop of Corila Research Program 2002–2004, Co.Ri.La., Venice, Italy.

McCowan, J. (1891), On the solitary wave, *Philos. Mag.*, *36*, 430–437.

Padilla-Hernàndez, R., and J. Monbaliu (2001), Energy balance of wind waves as a function of the bottom friction formulation, *Coastal Eng.*, *43*, 131–148.

Phillips, O. M. (1957), On the generation of waves by turbulent wind, *J. Fluid Mech.*, *2*, 417–445.

Phillips, O. M. (1966), *The Dynamics of the Upper Ocean*, Cambridge Univ. Press, New York.

Resio, D. T. (1987), Shallow-Water Waves. I: Theory, *J. Waterw. Port Coastal Ocean Eng.*, *113*, 264–281.

Resio, D. T., and W. Pierre (1989), Implication of an f^{-4} equilibrium range for wind generated waves, *J. Phys. Oceanogr.*, *19*, 193–204.

Ris, R. C., L. H. Holthuijsen, and N. Booij (1999), A third-generation wave model for coastal regions: 2. Verification, *J. Geophys. Res.*, *104*, 7667–7681.

Schwab, D. J., J. R. Benett, P. C. Liu, and M. A. Donelan (1984), Application of a simple numerical wave prediction model to Lake Erie, *J. Geophys. Res.*, *89*, 3586–3592.

Smith, S. D., and E. G. Banke (1975), Variation of the sea surface drag coefficient with wind speed, *Q. J. R. Meteorol. Soc.*, *101*, 665–673.

Snyder, R. L., R. B. Long, F. W. Dobson, and J. A. Elliott (1978), The Bight of Abaco pressure experiment, in *Turbulent Fluxes Through the Sea Surface, Wave Dynamics and Prediction*, edited by A. Favre and K. Hasselmann, Springer, New York.

Soulsby, R. L. (1995), Bed shear-stresses due to combined waves and currents, in *Advances in Coastal Morphodynamics*, edited by M. J. F. Stive et al., pp. 4-20–4-23, Delft Hydraul., Delft, Netherlands.

Soulsby, R. L. (1997), *Dynamics of Marine Sands: A Manual for Practical Applications*, 248 pp., Thomas Telford, London.

Umgiesser, G., and A. Bergamasco (1993), A staggered grid finite element model of the Venice lagoon, in *Finite Elements in Fluid: New Trends and Applications*, edited by K. Morgan et al., pp. 659–668, Pineridge, Swansea, U. K.

Umgiesser, G., M. Sclavo, and S. Carniel (2002), Modeling the bottom stress distribution in the Venice lagoon, in *Scientific Research and Safeguarding of Venice, Corila Research Program 2001 Results*, pp. 287–299, Corila, Venice, Italy.

Umgiesser, G., M. Sclavo, S. Carniel, and A. Bergamasco (2004), Exploring the bottom stress variability in the Venice lagoon, *J. Mar. Syst.*, *51*, 161–178.

Willmarth, W. W., and C. E. Wooldridge (1962), Measurements of the fluctuating pressure at the wall beneath a thick turbulent boundary layer, *J. Fluid Mech.*, *14*, 187–210.

Wood, D. J., M. Mattray, and H. Oumeraci (2001), The SWAN model used to study wave evolution in a flume, *Ocean Eng.*, *28*, 805–823.

L. Carniello, L. D'Alpaos, and A. Defina, Department IMAGE, University of Padova, Via Loredan 20, 35131 Padua, Italy. (carniello@idra.unipd.it; dalpaos@idra.unipd.it; andrea.defina@idra.unipd.it)

S. Fagherazzi, Department of Geological Sciences and School of Computational Science and Information Technology, Florida State University, Tallahassee, FL 32306-4120, USA. (sergio@idra.csit.fsu.edu)